

# Topographic evidence for recent intraplate reactivation in NW Uruguay

Mauricio B. Haag<sup>1,2\*</sup>, Lindsay M. Schoenbohm<sup>1,2</sup>, Rossano Dalla Lana Michel<sup>3</sup>,  
Claiton M. dos Santos Scherer<sup>3</sup>, Gerardo Veroslavsky<sup>4</sup>, Josefina Marmisolle<sup>5,6</sup>

<sup>1</sup> Department of Earth Sciences, University of Toronto, Toronto, ON, Canada

<sup>2</sup> Department of Chemical and Physical Sciences, University of Toronto Mississauga, Mississauga, ON, Canada

<sup>3</sup> Instituto de Geociências, Universidade Federal do Rio Grande do Sul, Porto Alegre, RS, Brazil

<sup>4</sup> Facultad de Ciencias, Universidad de la República, Montevideo, MO, Uruguay

<sup>5</sup> PEDECIBA Geociencias, Universidad de la República, Montevideo, MO, Uruguay

<sup>6</sup> Transición Energética, ANCAP, Montevideo, MO, Uruguay

\* Corresponding author: [mauricio.haag@mail.utoronto.ca](mailto:mauricio.haag@mail.utoronto.ca)

Mauricio B. Haag (<https://orcid.org/0000-0001-5038-4418>)

Lindsay M. Schoenbohm (<https://orcid.org/0000-0001-7898-356X>)

Rossano Dalla Lana Michel (<https://orcid.org/0000-0001-7767-6189>)

Claiton M. dos Santos Scherer (<https://orcid.org/0000-0002-7520-1187>)

Gerardo Veroslavsky (<https://orcid.org/0000-0002-9121-4666>)

Josefina Marmisolle (<https://orcid.org/0009-0005-1313-263X>)

## Key points:

- Topographic and field data uncovers evidence for recent tectonic activity in Uruguay.
- Deformational features include fault scarp and offset streams, compatible with normal and strike-slip deformation.
- Recent deformation matches location and orientation of ancient (Proterozoic and Mesozoic) inherited structures.

## **Abstract**

Located in eastern South America, Uruguay has been considered tectonically inactive since rifting in the Cretaceous. Here, we use a high-resolution digital elevation model (DEM) and field observations to investigate the presence of recent tectonic activity in the Basaltic Plateau, northwest Uruguay. Based on topographic-, drainage network- and field-based data, we identify evidence for long-lasting, and potentially ongoing/recent (Cretaceous-Cenozoic) tectonic deformation, including fault breccia, scarps, and offset channels, indicative of potential normal and strike-slip deformation. The orientation and spatial pattern of this deformation aligns closely with inherited structures, particularly Proterozoic and Mesozoic fault zones. Our results suggest that reactivation of ancient basement structures has localized recent deformation, highlighting the importance of tectonic inheritance in controlling deformation in intraplate regions considered otherwise tectonically “inactive”. The detection of subtle, recent deformation in Uruguay is only possible because of high-resolution topographic data, underscoring the role of modern remote sensing tools in assessing tectonic activity in presumed stable regions. Lastly, this study highlights the need to reassess intraplate landscapes for signs of recent deformation, particularly in regions underlain by major basement structures that may act as zones of weakness, facilitating deformation even under minor stress conditions.

## 1. INTRODUCTION

Traditionally viewed as tectonically quiescent, intraplate landscapes are increasingly recognized as sites of subtle but geologically significant deformation ([Salomon et al., 2015a, b](#); [Muir et al., 2023](#)). In many passive margins and cratonic settings, an increasing number of studies show that ancient zones of weakness, such as shear zones and lithospheric scars, can influence tectonics, present-day topography and drainage architecture long after the cessation of major tectonic activity ([Heron et al., 2016](#); [Salomon et al., 2015a, b](#); [Fontainha et al., 2021](#)). These inherited structures can be reactivated under far-field stress regimes, producing deformation patterns that are easily overlooked or hard to recognize in low-relief terrains (e.g., [Giona Bucci and Schoenbohm, 2022](#)).

Located in South America, the Basaltic Plateau in northwestern Uruguay features extremely flat topography characterized by relief less than  $<35$  m/km ([Kröhling et al., 2014](#)). This landscape is underlain by an extensive sequence of Cretaceous basalts partially overlying sedimentary rocks of the Paraná basin, both emplaced atop a complex Precambrian basement that includes several major Proterozoic shear zones ([Passarelli et al., 2011](#); [Oriolo et al., 2018](#)). Although typically classified as tectonically stable, historical seismicity and recent geophysical studies suggest that this region remains sensitive to changes in the far-field stress regime imposed by the Andean orogeny ([Baxter and Smith, 2020](#)). Furthermore, the Basaltic Plateau features extensive topographic lineaments ([Marmisolle et al., 2016](#); [Blanco et al., 2021](#)) and fluvial network anomalies commonly associated with structural control and recent tectonic activity ([Sánchez Bettucci et al.,](#)

2025). Despite these observations, the relationship between topography, drainage network geometry, underlying structural inheritance and potential tectonic reactivation in this region remains poorly understood.

In this study, we combine high-resolution topographic analysis with field-based structural observations to investigate if the reactivation of ancient shear zones controls the geomorphic evolution of the Basaltic Plateau in NW Uruguay, and if so, how. Our findings suggest recent deformation in this region, with normal and strike-slip deformation along pre-existing NW-SE and ENE-WSW-trending structures. Structural lineaments exert strong control over drainage pattern and orientation, and control the occurrence of minor (up to 10 m) fault scarps, offset channels and incised valleys. These patterns suggest ongoing reorganization of fluvial systems as a result of this deformation, and therefore indicate some degree of tectonic activity in the area. Our findings contribute to a growing body of evidence suggesting that intraplate regions are subject to subtle tectonic signals in settings otherwise considered tectonically dead.

## 2. GEOLOGICAL SETTING

In this study, we focus on a low-relief surface known as the Basaltic Plateau located in NW Uruguay ([Fig. 1a](#)) ([Kröhling et al., 2014](#)). The Basaltic Plateau features extremely low relief (typically less than 35 m/km) and maximum surface elevation of up to 350 m asl ([Fig. 1b](#)). Located more than 500 km away from the Atlantic coast, this area has been considered largely tectonically inactive since the opening of the South Atlantic Ocean ca. 120 Ma

(Panario et al., 2014). To the east, the Basaltic Plateau is bounded by a regional escarpment along the Negro River watershed, while to the west the Plateau gently grades to the Uruguay River, with an average regional slope of  $< 1^\circ$ .

Geologically, the Basaltic Plateau is mainly composed of volcanic rocks of the Paraná-Etendeka Large Igneous Provinces (Lower Cretaceous) emplaced in the Norte Basin (de Santa Ana, 1989), locally grouped into the Arapey Formation (Porta et al., 1985; de Santa Ana and Veroslavsky, 2003). The volcanics overlie sedimentary siliciclastic rocks of the Paraná Basin (de Santa Ana and Veroslavsky, 2003; Scherer et al., 2023), including fluvial-eolian and marine deposits (Amarante et al., 2019; Scherer et al., 2023; Manna et al., 2025). Recently, geochemical studies revealed the presence of Cenozoic (51 – 64 Ma) alkaline volcanic vents in the Basaltic Plateau (Muzio et al., 2022). These units both overlie the Nicolás Pérez and Piedra Alta basement terranes (Archean-Proterozoic; Oriolo et al., 2016), which were extensively deformed during Gondwana Amalgamation during the Proterozoic (Porta et al., 1985). These orogenies involved the accretion of several tectonic terrains and the development of notable, crustal-scale shear zones, mainly oriented along NW-SE and ENE-WSW trends (Passarelli et al., 2011; Oriolo et al., 2018).

Previous studies have mapped important lineaments traversing the Basaltic Plateau (Rodríguez et al., 2015; Marmisolle et al., 2016; Veroslavsky et al., 2019, 2021, 2024; Morales et al., 2021). Based on subsurface mapping including seismic, magnetotelluric, gravimetry and borehole interpretations (e.g., Rodríguez et al., 2015; Marmisolle et al., 2016; Morales et al., 2021; Veroslavsky et al., 2019, 2021, 2024), NW-SE and ENE-WSW-trending faults have

been shown to control both the deposition and deformation of the basement and overlying Mesozoic sequences, including the volcanic rocks of the Arapey Formation. (Figs. 1c, 2a and 2d; Marmisolle et al., 2016; Veroslavsky et al., 2019, 2021). Among these structures, the Lunarejo, Arroyo Las Cañas and Arapey/Sarandí del Yí Lineaments are the most prominent features in the study area, and are also observed in gravimetric maps (Fig. 2a).

Recent seismicity in Uruguay is concentrated in the Río de la Plata estuary (Baxter et al., 2021), although notable onshore earthquakes are documented (Sánchez Bettucci et al., 2025), mostly along the Sarandí del Yí Lineaments (Fig. 1a). Among these, the 1948 events ( $M_L$  5.8 and 5, and moment magnitude  $M_w$ , 5.8) are among the most significant events documented in onshore Uruguay (Baxter et al., 2021; Sánchez Bettucci et al., 2025), followed by the 1959 ( $M_L$  5.0) earthquake and more recent moderate events including the 1990 ( $M_L$  3.0) and the 2021 and 2022 ( $M_L$  3.7 and 3.9,  $M_w$  4.3) events (Fig. 1a; Baxter et al., 2021; Sánchez Bettucci et al., 2025).

### **3. METHODS**

#### **3.1. Inherited Structure, Lineament and Fluvial Network Analysis**

We use topographic data to investigate reactivation and recent tectonic activity in the Basaltic Plateau, including identifying topographic lineaments, drainage anomalies and potential fault escarpments (e.g., Li et al., 2022). To this end, we make use of two digital elevation models (DEMs): the 12.5 m/pixel ALOS-PALSAR from the ASF DAAC (JAXA, 2014; <https://search.asf.alaska.edu>) and the 2.5 m/pixel IDEuy from the *Infraestructura de Datos*

*Espaciales de Uruguay* (IDEuy, 2018). We conduct detailed topographic analyses along lineaments that exhibit evidence of vertical displacement, which may be used to estimate fault throw (Figs. 6 and 7).

Topographic lineaments guide erosion and fluvial network orientation at the surface and may reflect reactivation of inherited structures (e.g., Kirkpatrick et al., 2020). We use the 2.5 m/pixel IDEuy DEM to derive hillshade and slope maps for the study area. Hillshade maps are used to manually identify topographic lineaments using different illumination orientations (azimuth 045, 135, 225, and 315) at a 1:10,000 scale within the Basaltic Plateau. Combined with slope data, hillshade maps are also used to identify major, regional lineaments (Fig. 1a) and potential fault scarps. To assess the influence of topographic lineaments on drainage patterns, we analyzed stream orientations using 100 m-long river segments located within a 2-km buffer zone around each lineament (Supplementary Fig. 2). This analysis was conducted separately for different stream orders following the Strahler classification. Planform analysis of drainage networks provides valuable insights into lithological and tectonic controls on landscape evolution (Pereira-Claren et al., 2019). To examine drainage patterns and stream orientation we use TopoToolbox 2.3 (Schwanghart & Scherler, 2014) to extract the drainage network from the high-resolution IDEuy DEM. Then, we examine the drainage network for drainage anomalies (e.g., offset channels, barbed tributaries, deflected channels, faceted spurs, and incised valleys). River directions along the 0, 45, 90, and  $135 \pm 1^\circ$  azimuths were excluded due to artifacts introduced by the flow routing algorithm (see Supplementary Fig. 2).

We identified the presence of underlying inherited structures through a synthesis of existing geophysical and geological datasets for Uruguay, including seismic profiles, borehole data, gravimetry, and magnetometry. Gravimetric data from [Rodríguez et al. \(2015b\)](#) were used to delineate major structural lineaments across the study area ([Fig. 2a](#)). Although high-resolution magnetometry data are unavailable for the basaltic plateau itself, we incorporated data from the Uruguayan Shield located further south ([Nuñez Demarco et al., 2020](#)). Despite not being directly beneath the study area, the Uruguayan Shield belongs to the same structural province. Therefore, it is reasonable to expect that these regional lineaments extend northward into the Basaltic Plateau. Using datasets compiled by [Nuñez Demarco et al. \(2020\)](#), we extracted the orientations of Proterozoic and Mesozoic structural trends and major dike swarms within the Uruguayan Shield ([Fig. 2d](#)). These orientations provide a framework for interpreting structural inheritance in the overlying basaltic units. Additionally, borehole records and seismic sections from the basaltic plateau (e.g., [Marmisolle et al., 2016](#); [Veroslavsky et al., 2019, 2021, 2024](#)) offer direct subsurface evidence for structural lineaments ([Fig. 1a](#)).

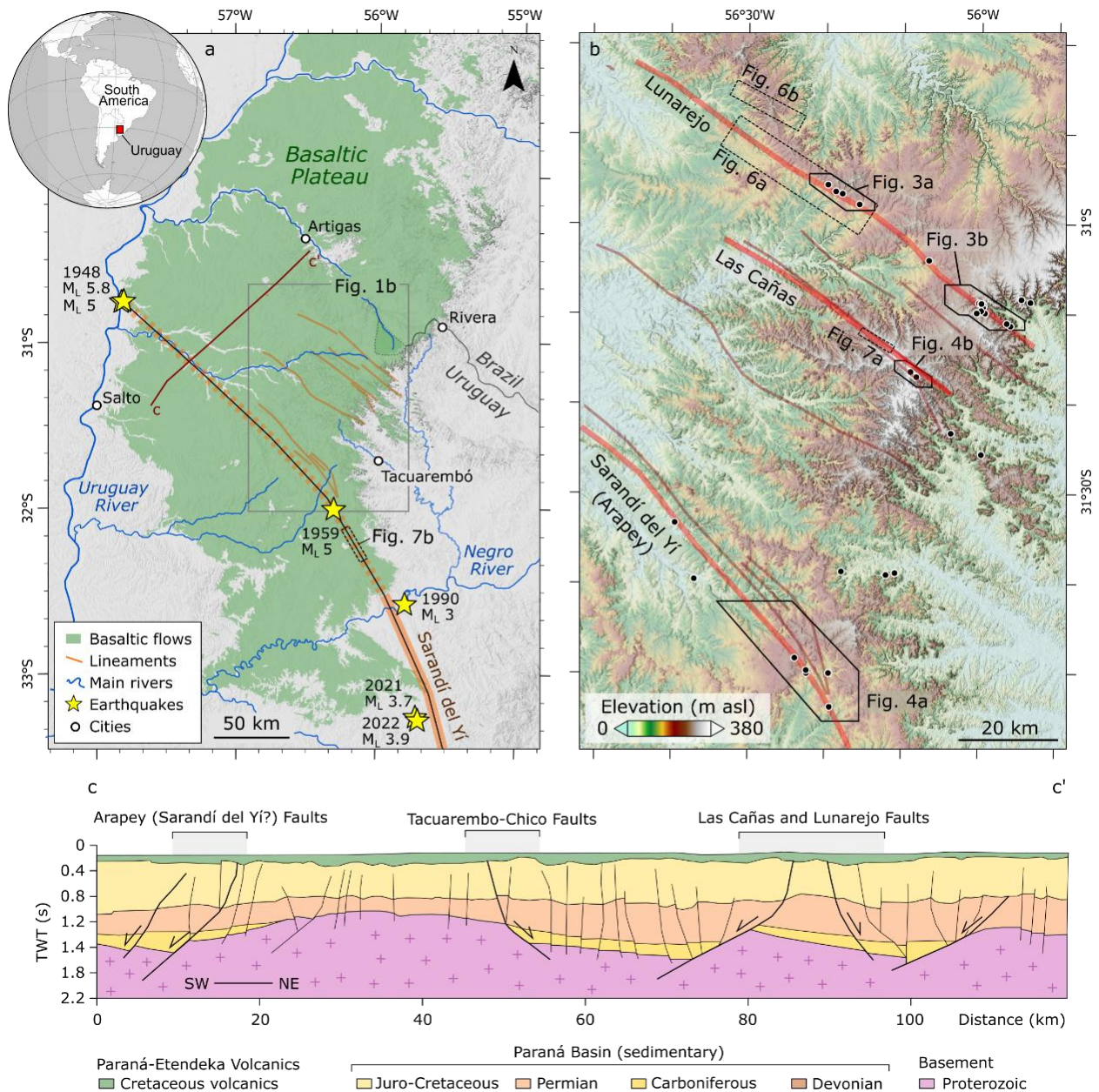


**Figure 1.** Study setting. (a) The basaltic plateau in NW Uruguay, with onshore earthquakes with local magnitude ( $M_L$ )  $\geq 3$  (Sánchez Bettucci et al., 2025). (b) Elevation map of the study setting, highlighting visited sites (black dots) and interpreted topographic lineaments. (c) NE-SW interpreted seismic section highlighting the presence of inherited structures in the Basaltic Plateau (adapted from Veroslavsky et al., 2021); TWT denotes two-way traveltime. Additional cross sections are provided in Supplementary Fig. 1.

### 3.2. Field observations and structural data collection

Outcrop scale fracture networks can be used to track deformation and gain insight into larger tectonic processes (Tibaldi et al., 2021; Panara et al., 2024). On the basis of our observations of topographic and drainage anomalies, we identified four field areas for additional study and validation (Fig. 1b). We examined these sites using a combination of outcrop and aerial photograph mapping of river channels and bedrock exposures. Note that despite the thin soil cover, the region is generally covered and of low relief, meaning that quality exposures are limited.

We collected aerial imagery with a UAV model DJI Mavic 2 Pro, which allowed us to obtain detailed images (Figs. 8 and 9) with a spatial resolution of ~ 1 mm/pixel. Using Agisoft *Metashape*, we generate an orthomosaic for each area and perform detailed lineament mapping on these outcrops. For each field area, we map fracture patterns, including orientations, length, and spacing (e.g., Peace and Jess, 2023). This analysis enables us to compare outcrop-scale fracture patterns with regional-scale structural lineaments.

To determine deformation patterns in the study area, we performed structural field measurements at 23 sites across these four field areas where we were able to identify good exposures of fractured bedrock (Figs. 3 and 4). We measured the orientations of fractures using an *iPad Mini 2* and the software *Climo* following the recommendations of Pascal (2022). We use *Stereonet 11* (Cardozo & Allmendinger, 2013) to process field data, which were grouped using stereonets, rose diagrams, and density plots. Due to the scarcity of kinematic

indicators in the examined outcrops, conducting a paleostress inversion was not feasible in the study area.

## 4. RESULTS

### 4.1. Lineament and stream orientation

Based on high-resolution DEMs, we mapped over 3,000 topographic lineaments in the study area (Fig. 2a). Our data demonstrate a predominant NW-SE trend ( $\sim 135^\circ$  azimuth) of lineaments in the region (Fig. 2a). This can be seen in the high density/frequency of lineaments with a NW-SE orientation (Figs. 2b, c) and in that lineaments of this orientation tend to be longer, reaching up to 6 km in length (Fig. 2b). This prominent NW-SE orientation is also seen in the orientation of segments of the stream network at all orders (Fig. 2c). There is a secondary trend of lineaments with an approximately ENE-WSW orientation ( $\sim 70^\circ$  azimuth; Figs. 2b, c). Interestingly, the stream network does not reflect this trend but rather shows alignment orthogonal to the main lineament direction (NE-SW). A tertiary trend of stream segments-oriented E-W ( $\sim 90^\circ$  azimuth) is most apparent only for higher order ( $> 3^{\text{rd}}$ ) streams (Fig. 2c).

The major surface lineaments we mapped using DEMs closely align with the orientations of subsurface structures inferred from gravimetric data (Nuñez Demarco et al., 2020; Fig. 2a). Ancient structural trends, spanning from the Proterozoic to the Mesozoic, show a predominance of N-S, NNE-SSW, and E-W orientations within Archean-Proterozoic basement (Fig. 2d; Nuñez Demarco et al., 2020). In contrast, Mesozoic dike swarms exhibit

WNW–ESE, NW–SE, and E–W trends. NW–SE and E–W trends are closely aligned with regional surface lineaments, as well as major river orientations (Fig. 2e).

The NW–SE trend in lineament orientation is apparent at a smaller scale of observation across the Basaltic Plateau as well, particularly along northern and southern Lunarejo (Figs. 3a and 3b), Arroyo Las Cañas (Fig. 4b), and Sarandí del Yí (Fig. 4a) lineaments. E–W to ENE–WSW lineaments are particularly common in the Lunarejo region, where these structures appear to control the development of river valleys (Supplementary Fig. 3). Locally, lineaments appear to influence and disrupt drainage patterns, as evidenced by the rectangular planform of fluvial network observed in these regions (Fig. 5).

#### **4.2. Drainage reorganization and topographic evidence for deformation**

Inspection of drainage patterns and topography along major lineaments reveals the presence of fault scarps, offset channels, and divides that are consistent with fluvial network reorganization near topographic lineaments (Fig. 5) (e.g., Duvall and Tucker, 2015). For example, just north of the Lunarejo Lineament, offset channels are compatible with either top down to the NE displacement along a dip-slip fault or right-lateral displacement (Fig. 5a,b). This region also features growing channels with decreasing drainage toward the leading edge of lineament (Fig. 5b; Duvall and Tucker, 2015), compatible with right-lateral displacement. Along the Lunarejo Lineament, a potential fault scarp separates incised from non-incised fluvial valleys, indicating dip-slip faulting (Fig. 5c,d). Further south along the same lineament, the Lunarejo Valley features offset channels compatible with left-lateral displacement (Fig. 5e-g). Although interpretation of strike-slip disruption of drainage

networks is complicated, the upstream nature of displacement in some of these examples (Fig. 5f) supports this interpretation. Similarly, scarps are also present along the Arroyo Las Cañas Lineament, with minor vertical displacements (Fig. 5h,i). In the Sarandí del Yí Lineament, a wide (~ 50 m) valley is developed parallel to the lineament strike, denoting enhanced erosion along NW-SE lineaments (Fig. 5j,k).

Detailed topographic profiles from lineaments reveal minor vertical displacements, compatible with throw measurements of 2.9 – 5.1 m in the northern Lunarejo segment (Fig. 6a). In the middle part of the Lunarejo lineament, where vertical displacements are observed on opposite sides of the lineament (Fig. 5a), estimated throw measurements are highly variable, ranging from 6.3 – 11.2 m (Fig. 6b). The apparent reversal of throw along strike likely reflects strike-slip displacement and horizontal offset of topographic features, possibly in a right-lateral sense, rather than a change in dip-slip displacement. Further south in the study area, the Las Cañas lineaments features throw estimates of 6.9 – 12 m, including displacements along a subsidiary structure (Fig. 7a). Similarly to along the Lunarejo lineament (Fig. 6b), throw estimate along the Sarandí del Yí Lineament are highly variable and occur on opposite sides of the lineament, possibly also indicating right-lateral displacement along a strike-slip fault (Fig. 7b). Slope measurements along topographic profiles are reported in Supplementary Figs. 4 and 5.

### 4.3. Field observations

The Basaltic Plateau is characterized by extensive flat to gently sloping surfaces, with minimal (< 5 m) fluvial incision observed near the headwaters. Soil cover is generally thin (<

1 m), and sparse, small bedrock outcrops can be located across the study area (Fig. 8a, c). In contrast, relatively deeply incised channels (~50 m) dominate the landscape of the eastern escarpment in the Lunarejo Valley region (Fig. 8b). Notably, these channels are predominantly devoid of sediment (Supplementary Fig. 6).

Field inspection along major lineaments identified in DEMs (Fig. 2) reveals the presence of a strong association between topographic lineaments, fractured bedrock, and river channels (Fig. 8). In the northern segment of the Lunarejo Lineament (Fig. 8a), a major NW-SE lineament is associated with linear depressions in the field (Fig. 8a). Inspection of these features reveals thin soil underlain by extensively fractured and weathered bedrock (Supplementary Fig. 7). In the Lunarejo region (Fig. 8b), NW-SE lineaments are associated with incised (~ 50 m), linear valleys (Fig. 8b). Along the projected trace of the Sarandí del Yí shear zone (Fig. 8c) we observe a linear, fluvial depression. In this region, a series of closed depressions, similar to those observed in the Norther Lunarejo lineament region, are also present, but here at larger scale.

High-resolution UAV images reveal extensively fractured basaltic flows across all examined regions (Fig. 9). Fractures identified at outcrop scale using UAV generally align with major structural features, with a dominance of NW-SE and ENE-WSW-trending structures (Fig. 9). Locally, NW-SE fracture sets control the orientation of drainage networks, as exemplified in bedrock rivers along the Lunarejo Lineament (Fig. 9a). Although NW-SE sets are the most prevalent, ENE-WSW fracture sets also appear prominently in several regions (Fig. 9b-c). Along the Las Cañas Lineament (Fig. 9d), UAV imagery reveals fracture sets

consistent with shear along NW–SE planes, including the development of Riedel shears indicating a right-lateral sense of shear (9e-f). In the southern Sarandí del Yí Lineament, NNW-SSE sets dominate, largely following the inflection of the Sarandí del Yí Lineament observed toward the south of the study area (Fig. 1a).

The most common deformational features in the Basaltic Plateau are fractures (Fig. 10a-c) (sensu Pascal, 2022). Extensional (mode I) fractures are the most common structures, including joints and veins, which are typically filled with calcite and quartz. Extensional fractures are vertical, with spacing ranging from 5 – 15 cm (Fig. 10a-c). In addition to fractures, basaltic breccia and fault gouge are also observed in two locations, along the Lunarejo (Fig. 10d) and the Sarandí del Yí Lineament (Fig. 10e,f). In both cases, the location of fault gouge coincides with the location of major topographic lineaments (Figs. 3 and 4). Basaltic gouge and breccia are marked by the presence of alteration seams, calcite veins and zeolite surrounding relatively unaltered basaltic clasts, ranging from mosaic to crackle breccia (Woodcock and Mort, 2008). In a few locations, a secondary set of WNW-ESE-trending fractures is also observed cutting through fault gouge seams (Fig. 10e), suggesting at least two deformation phases. Striations and other slip indicators are rare in the study area (Fig. 10f,g), with occurrences primarily concentrated in the Lunarejo region. Where observed, these features indicate both dip-slip and strike-slip kinematics along NW-SE-trending structures (Fig. 3b).

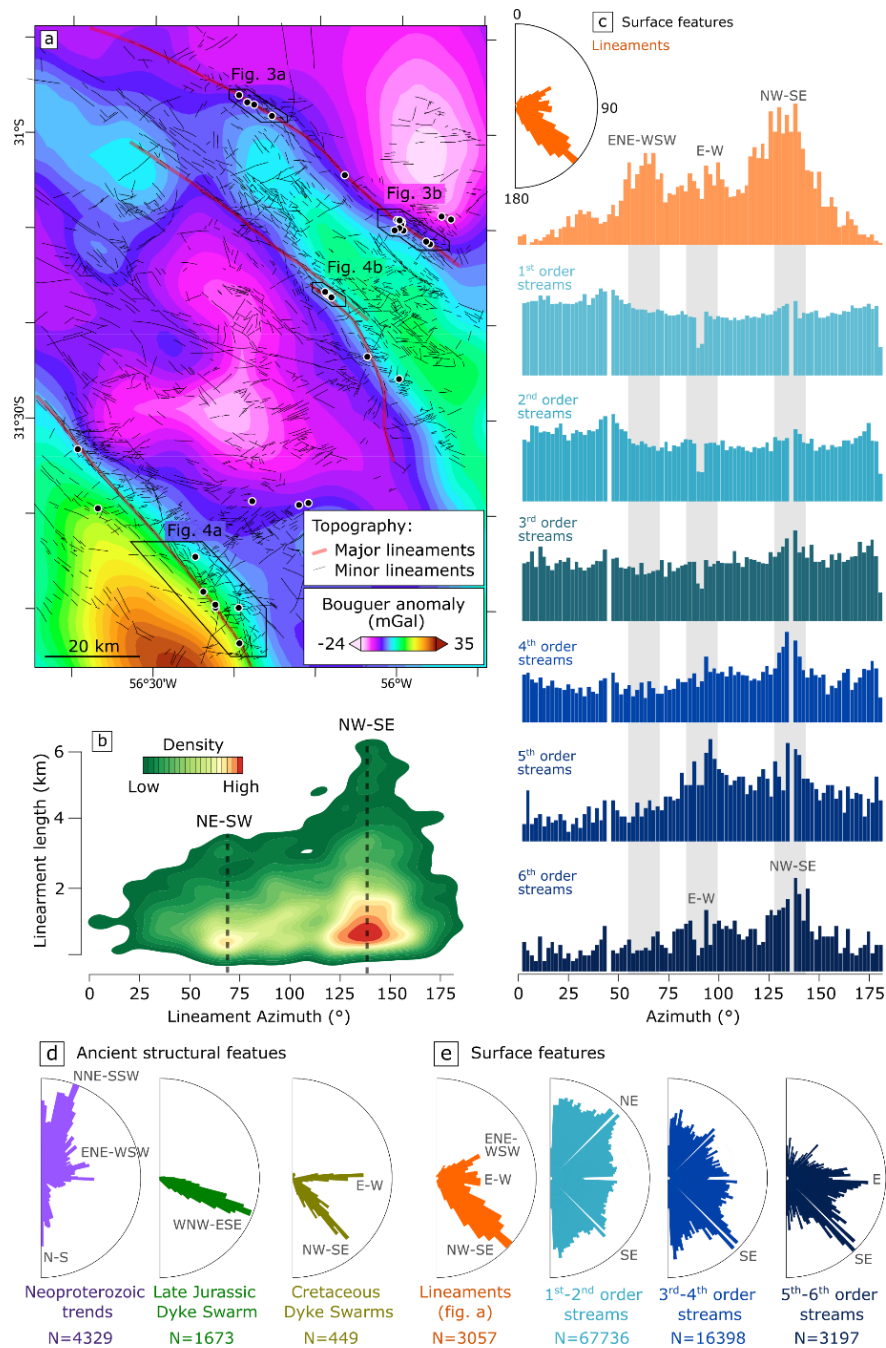


**Figure 2.** Lineament orientation and length. (a) Lineament distribution map underlain by Bouguer anomaly map (Rodríguez et al., 2015b). (b) Density diagram of lineament orientation vs. length. (c) Lineament and river orientation histograms. ENE-WSW, E-W, and NW-SE orientations are highlighted. Rose diagrams of (d) ancient structural trends mapped in the Uruguayan shield (Nuñez Demarco et al., 2020) and (e) present-day surface features. N indicates the number of measured structures.

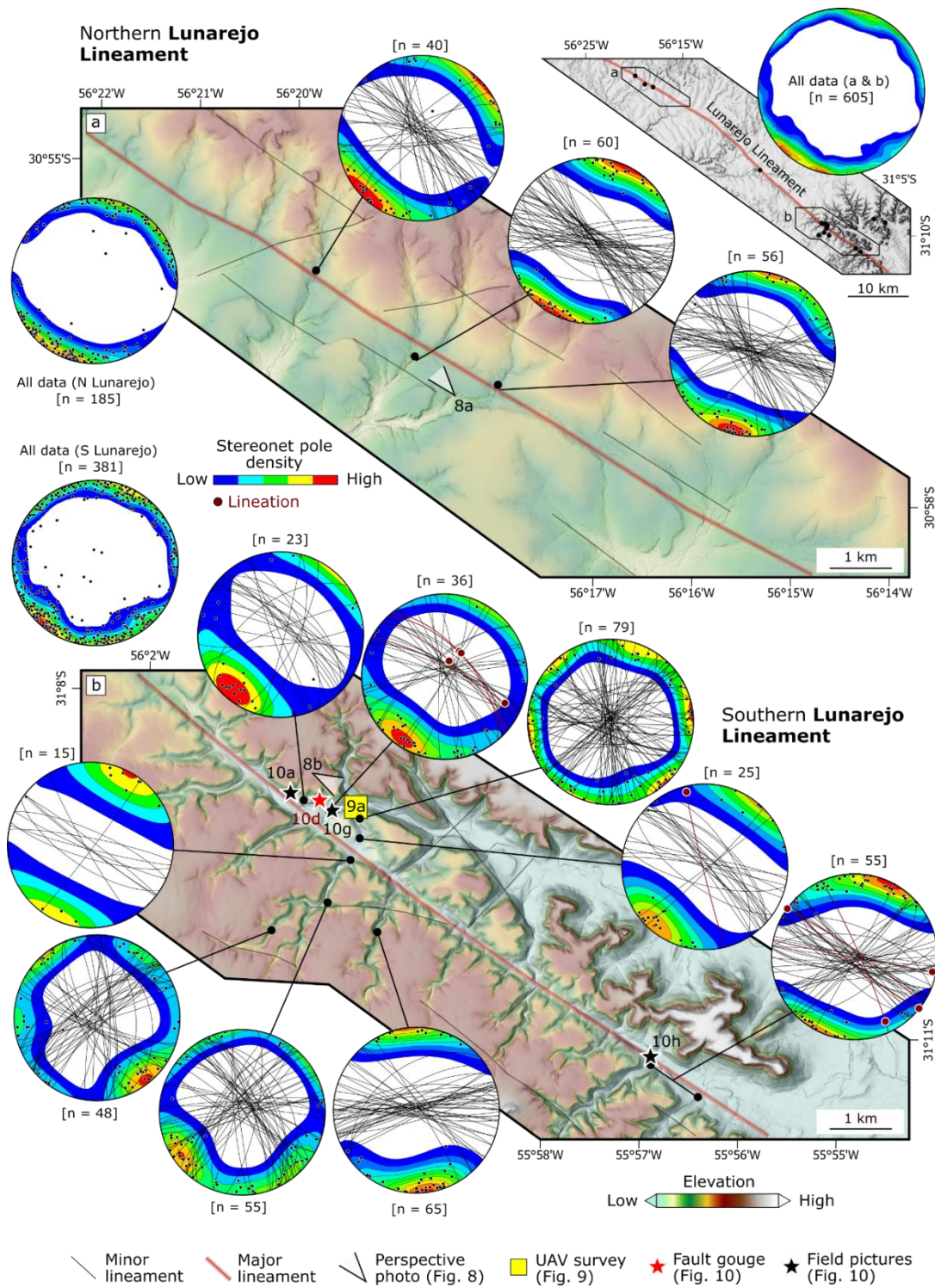


**Figure 3.** Lunarejo Lineament. a) northern section of the Lunarejo Lineament, with three measured sites. b) southern section of the Lunarejo Lineament, with a total of nine sites. Locations shown in Figs. 1b and 2a.

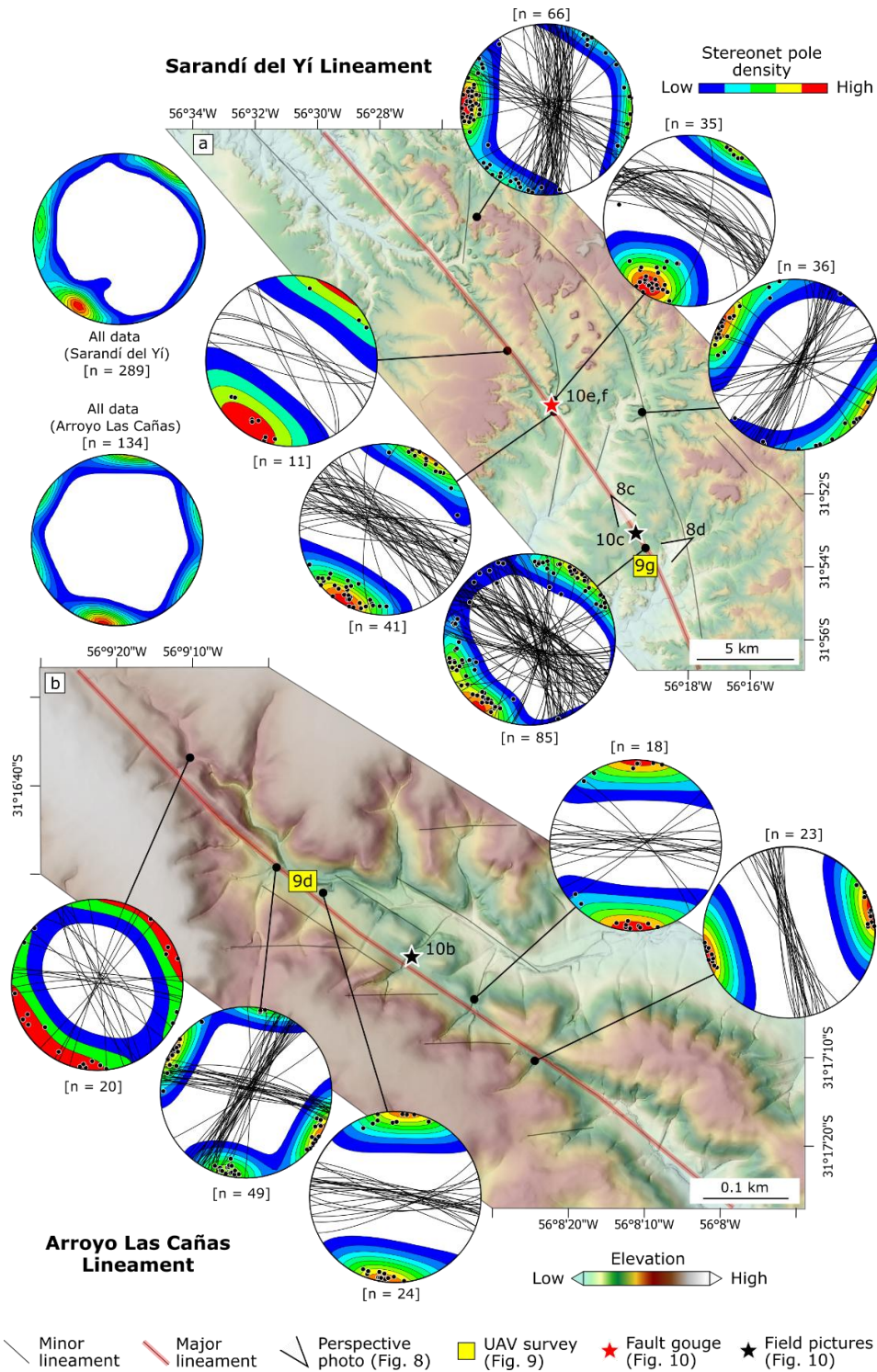


**Figure 4.** a) Sarandí del Yí Lineament, with seven measured sites. b) Arroyo Las Cañas Lineaments, with a total of five sites. Locations shown in Figs. 1b and 2a.

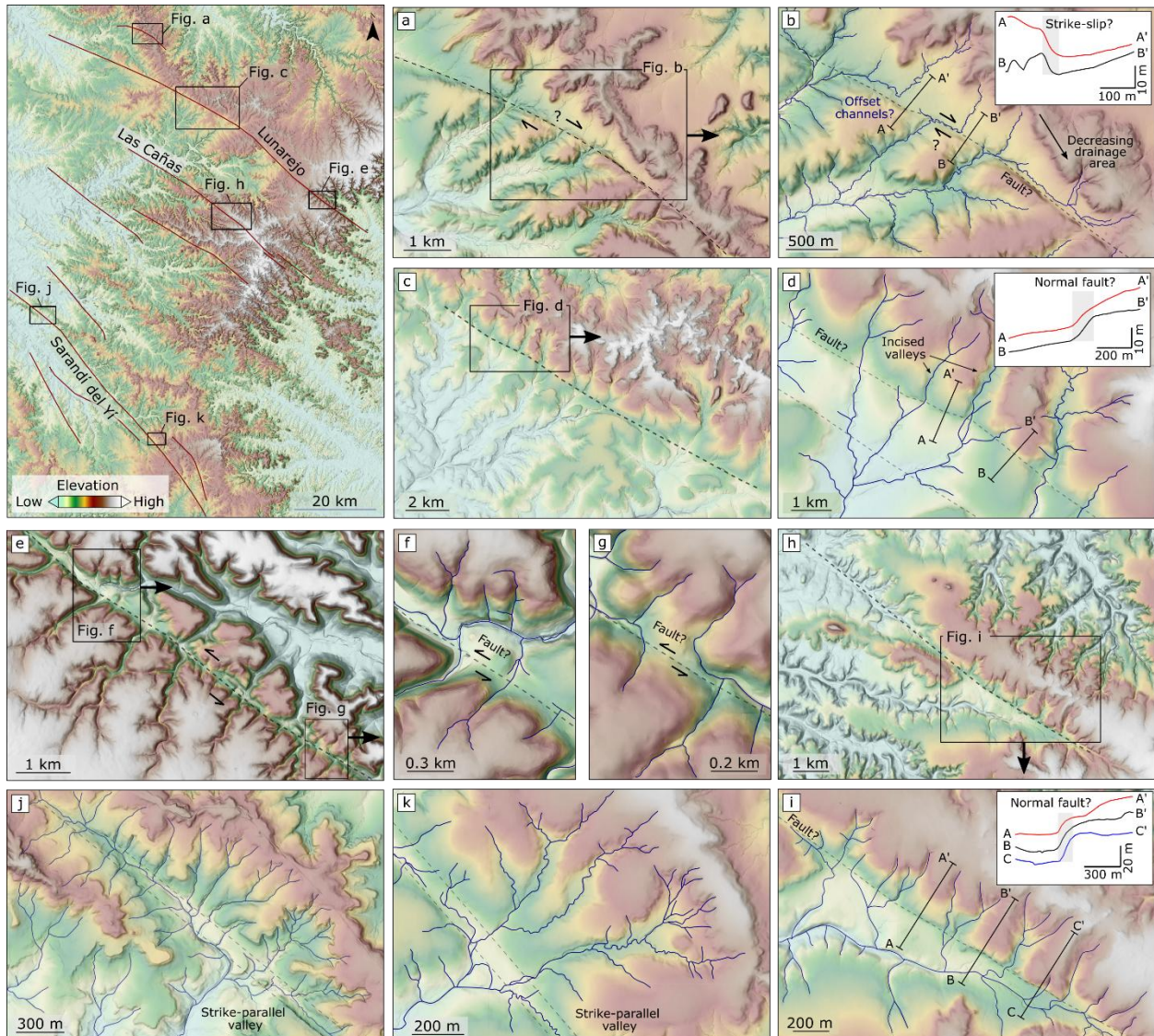


**Figure 5.** Potential evidence for drainage reorganization as response to tectonics in the Basaltic Plateau. (a-b) Offset channels and fault scarp in subsidiary structure near the northern Lunarejo Lineament; (c-d) Fault scarps and differential incision in the northern Lunarejo Lineament; (e-g) Potential offset channels along the southern Lunarejo Lineament; (h-i) Fault scarps and differential incision in the northern Las Cañas Lineament. (j-k) concentrated/preferential incision along NW-SE-trending river valleys. Locations of (a-j) are shown in the upper left inset.

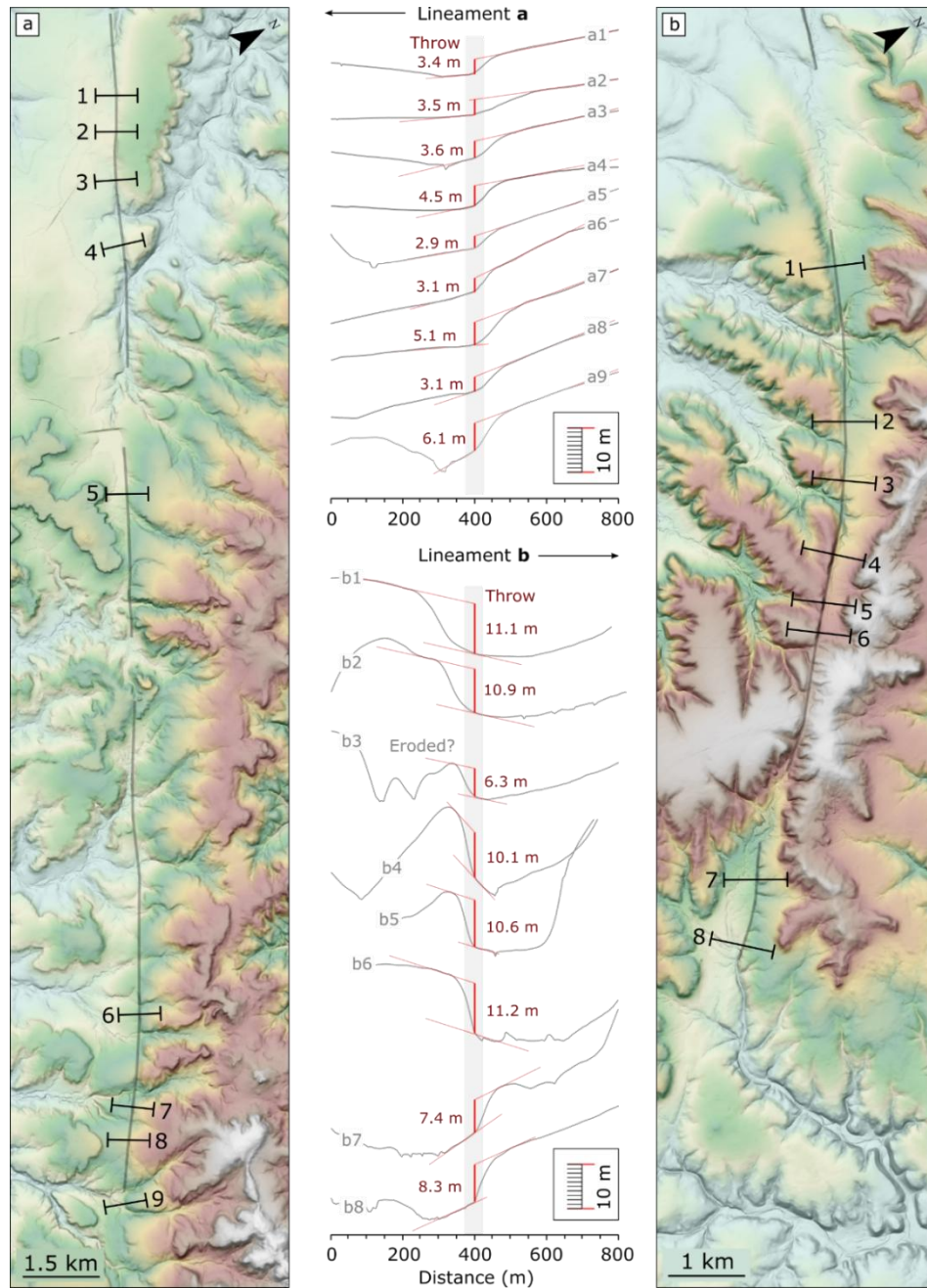


**Figure 6.** Topographic profile along potential fault traces in the Basaltic Plateau obtained using the high-resolution (2.5 m/pixel) DEM (IDEuy, 2018). (a) Northern Lunarejo Lineament, featuring throw measurements up to ~6 m. (b) ~10 km north of the northern Lunarejo Lineament, featuring throw estimates between 6 – 12 m; location shown in Fig. 1b.

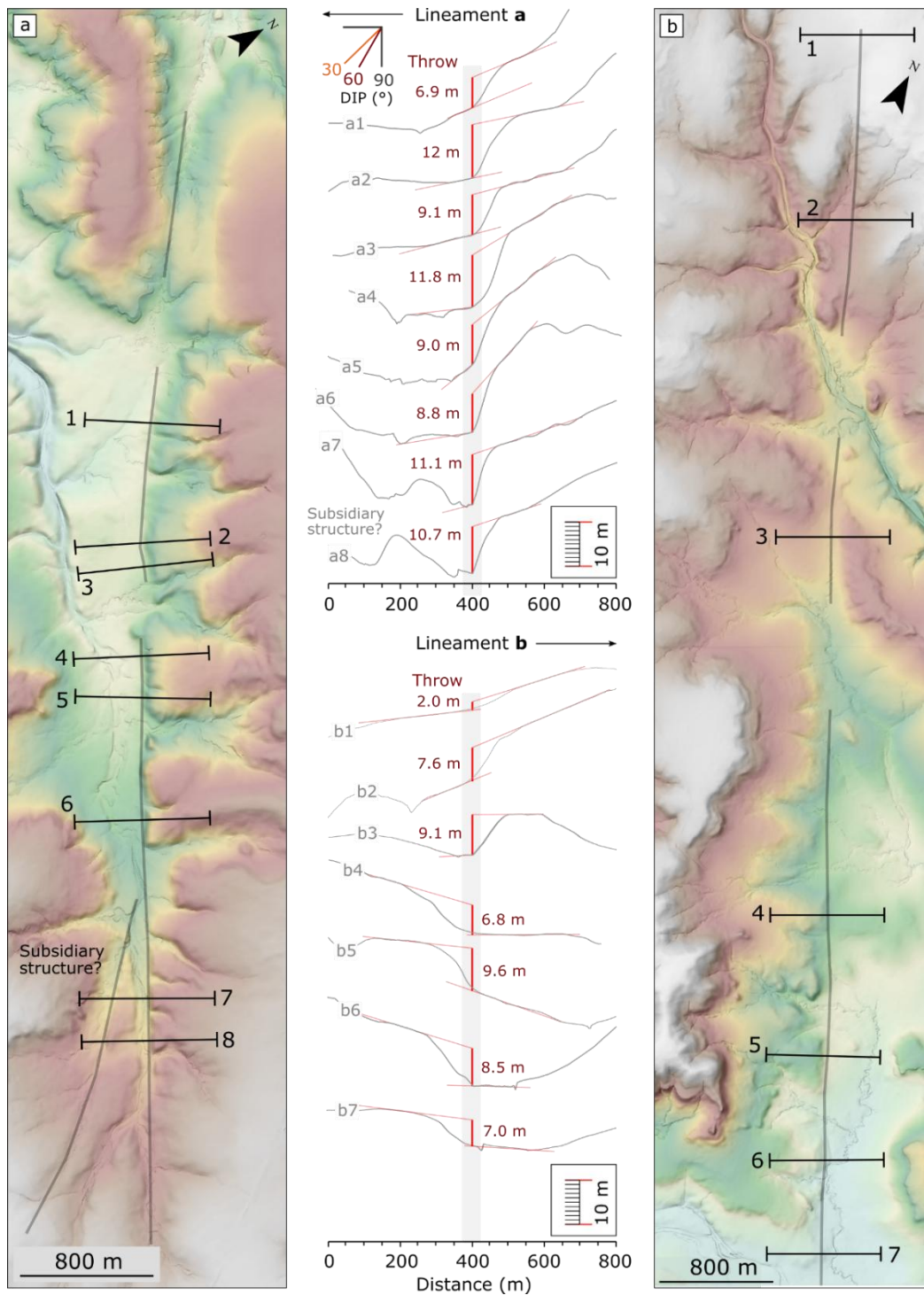


**Figure 7.** Topographic profile along potential fault traces in the Basaltic Plateau obtained using the high-resolution (2.5 m/pixel) DEM (IDEuy, 2018). (a) Las Cañas Lineament, featuring throw measurements between

7 – 12 m; location shown in Fig. 1b. (b) Southern segment of the Sarandí del Yí Lineament, featuring throw estimates between 2 – 10 m; location shown in Fig. 1a.

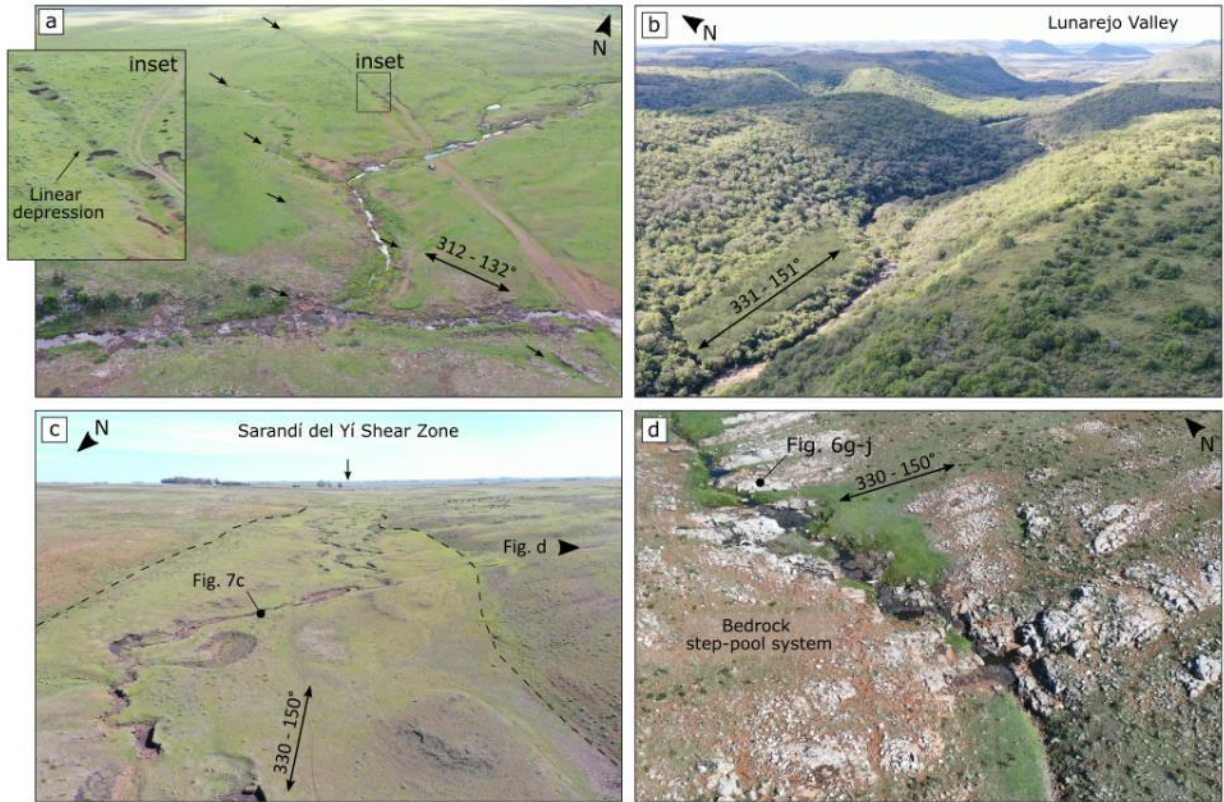


**Figure 8.** Field aspects of topographic lineaments. (a) Circular depressions along lineament trace in the northern Lunarejo Lineament (location in Fig. 3a); (b) Incised fluvial valley in the southern Lunarejo Valley (location in Fig. 3b); (c) Fluvial system overlapping the Sarandí del Yí Shear Zone (location shown in Figure 4a). (d) Extensively fractured bedrock along the channel walls, with a step-pool system (location shown in Figure 4a).

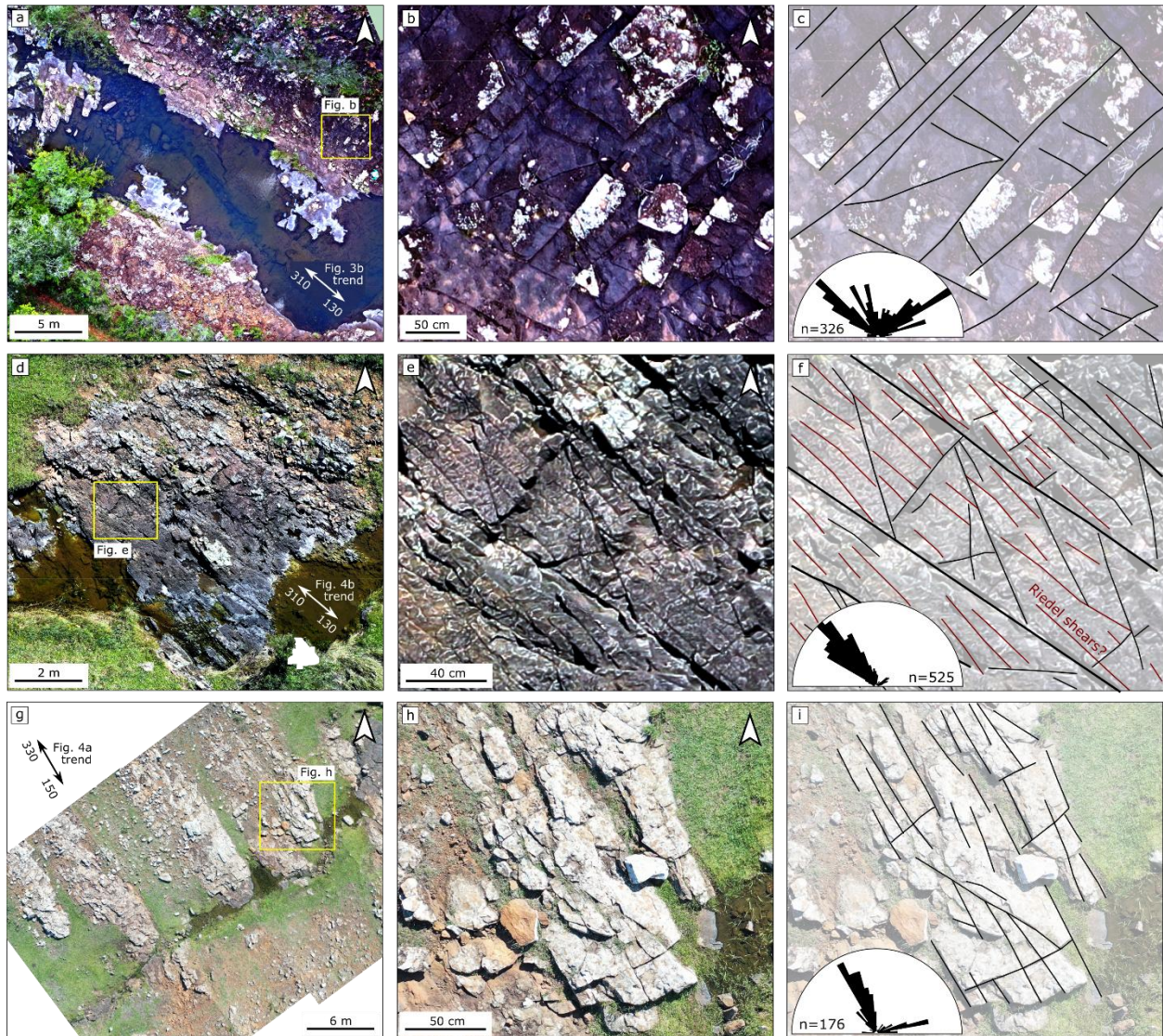


**Figure 9.** UAV observations and detailed fracture analysis. (a-c) Bedrock exposure along the Lunarejo Valley depicting a NW-SE fracture sets, with respective structural interpretation; location shown in Fig. 3b. (d-f) Bedrock exposure along the Las Cañas region, with respective structural interpretation; location shown in Fig. 4b. (g-j) Bedrock exposure in the Tacuarembó region (Sarandí del Yí lineaments) depicting a NNW-SSE fracture sets, with respective structural interpretation; location shown in Fig. 4a.

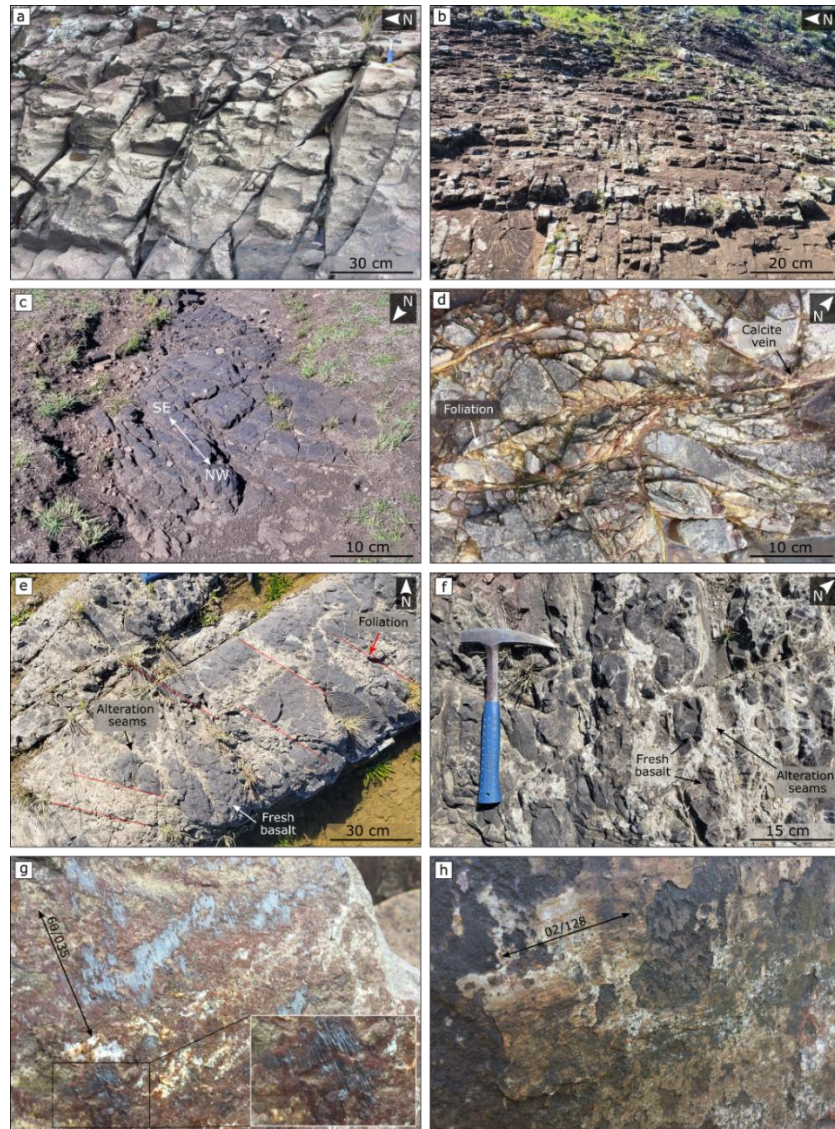


**Figure 10.** Deformational features in the field. (a) Irregular, nearly-vertical E-W trending structures (Fig. 3a). (b) Closely-spaced vertical E-W trending structures. (c) Closely-spaced NW-SE trending fractures along the Sarandí de Yí lineament (Fig. 4a). (d) Crackle basaltic breccia and fault gouge along bedrock exposure in the Lunarejo Valley (Fig. 3b). (e) Mosaic basaltic breccia and fault gouge along bedrock exposure along the Sarandí de Yí lineament (Fig. 4a). (f) Detailed features of fault gouge observed in (e), featuring alteration seams and fresh basaltic clasts (Fig. 4a). (g) High-plunging lineations in NW-SE-trending plane. (h) Nearly horizontal lineations in NW-SE-trending plane.

## 5. Discussion

### 5.1. Deformation style

Lineament analysis reveals that post-emplacement deformation is primarily concentrated along narrow (< 50 m) NW-SE-trending lineaments, and subordinate ENE-WSW-oriented structures (Fig. 2). In the field, deformation is mainly developed as fractures (Fig. 10a-c). Although these fractures could have several origins (e.g., cooling fractures, unloading fractures, tectonic fractures; Pascal, 2022), their length, consistent orientation, and alignment with major topographic lineaments (e.g., Fig. 3a, b and 4a) point to a tectonic origin. Cooling fractures typically occur at the scale of individual flows and are not expected to form laterally extensive, consistently oriented structures. Although cooling fractures are common in the Basaltic Plateau (see Supplementary Fig. 7), we did not incorporate these structures into our analysis. Similarly, unloading fractures, which tend to be vertical and reflect the modern stress field or topographic unloading, would be expected to vary in orientation according to topography (Moon et al., 2017). The consistent regional orientation and length of the lineaments is rather indicative of a tectonic origin. This hypothesis is supported by the presence of basaltic breccias and fault gouge in two locations along the Lunarejo Lineament (Fig. 10d) and in the vicinity of the Sarandí del Yi Lineament (Fig. 10e,f). The breccias mapped in NW Uruguay resemble basaltic breccias observed in fault zones in the Faroe Islands (e.g., Walker et al., 2013; Bamberg et al., 2023, their Fig. 2), Alaska (Braden and Behr, 2021), and Iceland (Karson et al., 2018), strengthening our interpretation of

displacement along some of these lineaments. Although rare, the presence of lineations (Fig. 10g,h) along major structures further supports this interpretation.

Secondly, topographic evidence, including throw measurements (Figs. 6 and 7), is consistent with dip slip, strike-slip, and/or oblique displacement along NW-SE lineaments (Figs. 6 and 7). While we cannot directly constrain the dip of these structures, the predominance of extensional features in the broader region (e.g., [Veroslavsky et al., 2021](#)) suggests that normal faulting is the most likely fault mechanism. For example, the presence vertical offsets compatible with throw measurements up to 12 m in the Lunarejo (Fig. 5c,d and 6a) and Arroyo Las Cañas (Fig. 5h-i and 7a) is broadly compatible with normal faulting (e.g., [Muir et al., 2023](#)). Additionally, the presence of offset channels located north of the Lunarejo lineament (Fig. 5a,b), in the Lunarejo Valley (Fig. 5e-g), and in the Arroyo Las Cañas region (Fig. 5h-i) provides geomorphic evidence for lateral (strike-slip) displacement along some lineaments in the Basaltic Plateau (Fig. 6b and 7b). However, in humid landscapes like NW Uruguay, channel responses to faulting are often diffuse and variable, and a mix of large and small offsets is expected in humid regions ([Reitman et al., 2019](#)), which can obscure topographic evidence for displacement. Therefore, the rarity of unambiguous displacement features, combined with potentially low deformation rates, limits our ability to precisely characterize these faults and accurately quantify displacement in the Basaltic Plateau. Despite extensive field mapping, the subdued topography, homogenous lithology, low tectonic rates, and chemical weathering in the Basaltic Plateau ([Garzanti et al., 2021](#)) pose

fundamental challenges to constraining fault kinematics and fully understanding the deformation history of this area.

## 5.2 Timing of deformation

### 5.2.1 Recent deformation

The lineaments, fractures, and fault-related features we observe in the Basalt Plateau must post-date emplacement of the Arapey basalts ca. 133 Ma ([Gomes and Vasconcelos, 2021](#)). Surface deformational features ([Fig. 5](#)) suggest recent/ongoing tectonic reactivation in the Basaltic Plateau. Unlike locations in the Atacama Desert, Mongolia and Namibia, where arid conditions can preserve fault scarps for tens of millions of years ([Muir et al., 2023](#)), the humid subtropical climate of Uruguay promotes intense chemical weathering ([Garzanti et al., 2021](#)), therefore shortening the preservation time of the surface expression of faults ([Reitman et al., 2019](#); [Li et al., 2021](#)). Further, in humid settings under low slip-rates, fault scarps may be rapidly eroded as a result from burial or erosion ([Marliyani et al., 2018](#)) and fault escarpments tend to be rapidly modified in humid climates ([Tucker et al., 2020](#)). In arid environments, the morphology of a scarp has been used as a relative indicator of formation age, with sharper, steeper slopes typically indicating more recent displacement ([Avouac, 1993](#)). The mapped fault scarp in the Basaltic Plateau feature slopes ranging from  $\sim 3 - 20^\circ$  (Supplementary Figs. 4 and 5), suggesting significant modification from initial escarpment geometry, which are expected to form at  $30 - 35^\circ$  ([Avouac, 1993](#)). Therefore, while it is difficult to precisely constrain the timing of deformation in NW Uruguay, the topographic preservation of fault traces points to relatively recent activity.

Geodetic and seismicity data support our interpretation of recent tectonic activity in the Basaltic Plateau. GPS data indicates that Uruguay is currently undergoing ESE-WNW directed horizontal shortening and NE-SW extension (Baxter and Smith, 2020), making NW-SE -trending structures prone to normal and strike-slip reactivation, consistent with our field observations. Further, recent seismic activity in the Basaltic Plateau has included  $M_L > 5$  events in 1948 and 1959 (Sánchez Bettucci et al., 2025). Historically, earthquakes with  $M_w$  up to 5.8 have been recorded in the Basaltic Plateau (Baxter et al., 2021), placing the area at lower end for potential surface rupture and fault scarp development (e.g., Muir et al., 2023).

#### 5.2.2 Post-breakup (Cenozoic) deformation

Although we find evidence for recent fault activity, considering the age of the examined rocks, the volcanic flows of the Basaltic Plateau could have recorded multiple episodes of deformation, from their emplacement to the present day. Evidence for multiple and/or recurrent episodes of deformation are provided by Cenozoic depositional patterns northwest of the study area, where NW-SE normal faults are shown to control the distribution of several sedimentary units throughout the Cenozoic (Veroslavsky et al., 2019; Blanco et al., 2021). Furthermore, compositional and geochemical data from these rock units suggest diagenetic processes, such as cement composition, compatible with faulting (Veroslavsky et al., 1997; Blanco et al., 2021).

Paleostress analyses indicate that the southeastern passive margin of South America has been predominantly under an E-W horizontal compressive regime since rifting (Cobbold et al., 2007; Salomon et al., 2015b). However, the widespread presence of normal faulting

documented by subsurface studies in the Basaltic Plateau ([Marmisolle et al., 2016, 2025](#); [Blanco et al., 2021](#); [Morales et al., 2021](#); [Veroslavsky et al., 2024](#)) indicates the presence of an E-W horizontal extensional regime at some point in this area. Additionally, both NW–SE and ENE–WSW-trending lineaments accommodate normal faulting (e.g., [Marmisolle et al., 2016, 2025](#); [Blanco et al., 2021](#); [Veroslavsky et al., 2024](#); [Fig. 1c](#)), suggesting that horizontal extension was not only pervasive but also structurally diverse. Although the precise timing of this extensional regime in northwestern Uruguay remains uncertain, horizontal neutral to extensional conditions in the Andes during the Late Paleocene–Early Eocene ([Horton, 2018](#)) possibly influenced the regional stress field in Uruguay (e.g., [Baxter and Smith, 2020](#)). In the Basaltic Plateau, Cenozoic horizontal extensional tectonics may be further supported by the presence of 51 – 64 Ma alkaline volcanic vents ([Muzio et al., 2022](#)), coinciding with the timing of extension in the Andes.

Furthermore, the oblique orientation of major tectonic structures relative to E-W horizontal compression recorded for most of the Cenozoic ([Salomon et al., 2015b](#); [Veroslavsky et al., 2021](#); [Baxter and Smith, 2020](#); [Sánchez Bettucci et al., 2025](#)) also facilitates the development of oblique and strike-slip deformation in the area. Particularly relevant to NW Uruguay, the Andean compressive climax in the Eocene-Oligocene (25 – 45 Ma) ([Bertin et al., 2025](#)) has been linked to the development of erosion surfaces in offshore Uruguay, suggesting far-field response of the margin to Andean tectonics ([Conti et al., 2023](#)). Based on these findings, we argue that NW Uruguay has been subject to

ongoing/intermittent intraplate deformation during most of the Cenozoic, including in modern times.

### 5.3 Structural inheritance

Post-rift deformation structures (including recent features) in the Basaltic Plateau exhibit predominantly NW-SE and ENE-WSW orientations, strongly matching the trends of ancient basement structures mapped across the region (Fig. 2; Nuñez Demarco et al., 2020). The consistent orientation between recent (this study), post-rift (Cenozoic) (Blanco et al., 2021; Veroslavsky et al., 2021, 2024; Marmisolle et al., 2025), and Mesozoic to Proterozoic (Milani and de Wit, 2008; Passarelli et al., 2011; Oriolo et al., 2018; Nuñez Demarco et al., 2020) structures strongly suggests the reactivation of pre-existing structures in NW Uruguay, highlighting the importance of tectonic inheritance in controlling post-breakup intraplate deformation.

These findings are supported by regional geological and geophysical studies in the area, which link the development of NW-SE-trending lineaments to Proterozoic Pan-African (NE-SW) and late Paleozoic to early Mesozoic Gondwanic (NW-SE) tectonic cycles (Fig. 2d; Milani and de Wit, 2008; Passarelli et al., 2011; Nuñez Demarco et al., 2020; Scherer et al., 2023; Veroslavsky et al., 2021, 2024). Additionally, structural reactivation is also documented in regions adjacent to the Basaltic Plateau, including examples from offshore Uruguay, where ancient NW-SE-structures control the formation of post-rifting depocenters (Marmisolle et al., 2025), as well as further northwest, in Argentina (Mira Carrión et al., 2015). Collectively, these findings indicate that NW-SE and ENE-WSW-trending structures are

regionally significant across the Parana Basin in Uruguay ([Veroslavsky et al., 2019, 2021, 2024](#)) and Brazil ([Milani and de Wit, 2008](#); [Scherer et al., 2023](#)), and potentially across South America ([Veroslavsky et al., 2021](#)).

Our findings are in agreement with post-breakup tectonic reactivation in other sections of the South American passive margin near the south Atlantic Coast in south Brazil ([Salomon et al., 2015b](#)). In this region, volcanic deposits display NNE-SSW-trending deformational features compatible with the orientation of underlying shear zones in the area ([Salomon et al., 2015b](#)). Across the South Atlantic, in Namibia, corresponding Etendeka flows feature similar post-breakup deformation patterns associated with the reactivation of preexisting shear zones ([Salomon et al., 2015a,b](#); [Muir et al., 2023](#)). These examples highlight the importance of inherited structures in localizing strain and accommodating tectonic reactivation in tectonically “inactive” intraplate settings.

Based on earthquake compilations, notable onshore earthquakes in Uruguay tend to concentrate along major lineaments, particularly the Sarandí del Yí Lineament ([Fig. 1a](#); [Sánchez Bettucci et al., 2025](#)). Although these earthquakes are relatively infrequent, their occurrence within the interior of the continent highlights the reactivation potential of inherited basement structures, particularly along major crustal lineaments such as those observed across the Basaltic Plateau ([Sánchez Bettucci et al., 2025](#)). This ongoing seismic activity indicates that inherited structures may remain mechanically weak, and therefore prone to reactivation under the current stress regime ([Baxter and Smith, 2020](#); [Sánchez Bettucci et al., 2025](#)).

#### 5.4. Intraplate tectonics and landscape evolution

The long-lived effects of crustal-scale structures, such as lithospheric scars and shear-zones, are known to control not only tectonic patterns ([Heron et al., 2016](#)) but also reactivation in otherwise “passive” settings (e.g., [Rimando and Peace, 2021](#)). Located at the margin of a major ancient Gondwanan structural zone, the Basaltic Plateau exhibits a prolonged history of tectonic reactivation, encompassing structures that date back to the Proterozoic ([Passarelli et al., 2011](#); [Oriolo et al., 2015, 2018](#)). Our analysis reveal that these ancient structural features continue to control surface expressions up to the present via reactivation. In the field, reactivated structures play a key role in concentrating deformation, leading to extensively fractured bedrock. This process is evidenced by the strong match between lineaments and stream orientation ([Fig. 2](#)), suggesting a correlation between fault damage and erodibility (e.g., [Kirkpatrick et al., 2020](#)).

Considering the tectonically stable setting of Uruguay, such deformation is unlikely to result from local tectonic activity alone. Rather, it might reflect the transmission of far-field stress from active plate boundaries, including the Andean orogeny. Indeed, modern GPS data reveals that the stress field in Uruguay is sensitive to Andean tectonic activity, with significant shifts in the stress field related to the 2010 Maule ( $M_w$  8.8) and the 2015 Illapel ( $M_w$  8.3) earthquakes in the Andes ([Baxter and Smith, 2020](#)).

As discussed in the previous section, mapped NW-SE striking structures in the Basaltic Plateau are prone to both normal faulting and both right- and left-lateral displacement under N-S to NNE-SSW horizontal extension. Although planform and hillslope

provide evidence of strike-slip deformation (e.g., offset channels and faceted spurs; Fig. 5), definitive indicators are sometimes ambiguous or absent along many sections of the potential fault traces. Furthermore, topography may not reliably reflect the current stress field in regions of structural reactivation. This is because deformation tends to localize along pre-existing weaknesses zones, favoring the reactivation of inherited structures rather than the formation of new structures (Zhou et al., 2013). Consequently, neotectonic interpretations based solely on surface morphology can be misleading, and deformation and seismicity will be concentrated along pre-existing fault zones (e.g., Rimando and Peace, 2021).

## 6. Conclusions

In this study we examine topographic, drainage and field data in the Basaltic Plateau in NW Uruguay to determine the presence of post-breakup tectonics in this region. Based on remote and field observations, we conclude that:

- Despite located in an intraplate setting, geomorphologic evidence suggests post-breakup (Late Cretaceous - Cenozoic) deformation in the Basaltic Plateau, including recent deformation.
- Deformation (fault scarps and offset channels) in the Basaltic Plateau is concentrated along major lineaments, particularly along the Lunarejo, Arroyo Las Cañas and Sarandí del Yí Lineaments (Figs. 5–7).
- Deformation is accommodated by normal and strike-slip faulting, in agreement with modern stress regimes (Baxter and Smith, 2020). Normal faulting is also compatible

with Paleocene – Eocene extensive to neutral condition in the Andean convergence ([Horton, 2018](#))

- Topographic lineaments follow two preferential trends, NW-SE and ENE-WSW ([Fig. 2](#)). Lineaments largely match the orientation of pre-existing basement structures developed during the Proterozoic Pan-African (NE-SW) and late Paleozoic to early Mesozoic Gondwanic (NW-SE) tectonic cycles ([Milani and de Wit, 2008](#); [Passarelli et al., 2011](#); [Veroslavsky et al., 2021](#)).
- Lineaments have a strong control on drainage pattern and orientation, indicating fault damage control on erodibility ([Kirkpatrick et al., 2020](#)). Rivers tend to develop along regional lineaments, which feature extensively fractured bedrock at an outcrop scale ([Fig. 9](#)).

## References

- ALOS PALSAR, Radiometrically and terrain-corrected digital elevation model (©JAXA, METI, 2014); <https://asf.alaska.edu>.
- Amarante, F.B., Scherer, C.M.S., Goso Aguilar, C.A., Reis, A.D. dos, Mesa, V., Soto, M., 2019. Fluvial-eolian deposits of the Tacuarembó formation (Norte Basin – Uruguay): Depositional models and stratigraphic succession. *Journal of South American Earth Sciences* 90, 355–376. <https://doi.org/10.1016/j.jsames.2018.12.024>
- Avouac, J., 1993. Analysis of scarp profiles: Evaluation of errors in morphologic dating. *J. Geophys. Res.* 98, 6745–6754. <https://doi.org/10.1029/92jb01962>
- Baxter, P., Bettucci, L.S., Costa, C.H., 2021. Assessing the earthquake hazard around the Río de la Plata estuary (Argentina and Uruguay): Implications for risk assessment. *Journal of South American Earth Sciences*. <https://doi.org/10.1016/j.jsames.2021.103509>
- Baxter, P., Smith, E.G.C., 2020. The contemporary strain rate field in Uruguay and surrounding region and possible implications for seismic hazard. *Journal of South American Earth Sciences*. <https://doi.org/10.1016/j.jsames.2020.102748>
- Bertin, D., Bustos, E., Grosse, P., Báez, W., 2025. The Central Andes of South America: A review of its tectono-magmatic evolution. *Journal of South American Earth Sciences* 158, 105503. <https://doi.org/10.1016/j.jsames.2025.105503>
- Braden, Z., Behr, W.M., 2021. Weakening Mechanisms in a Basalt-Hosted Subduction Megathrust Fault Segment, Southern Alaska. *JGR Solid Earth* 126. <https://doi.org/10.1029/2021jb022039>
- Cardozo, N., Allmendinger, R.W., 2013. Spherical projections with OSXStereonet. *Computers & Geosciences*. <https://doi.org/10.1016/j.cageo.2012.07.021>
- Cobbold, P.R., Rossello, E.A., Roperch, P., Arriagada, C., Gómez, L.A., Lima, C., 2007. Distribution, timing, and causes of Andean deformation across South America. *SP 272*, 321–343. <https://doi.org/10.1144/gsl.sp.2007.272.01.17>
- Conti, B., Novo, R., Marmisolle, J., Rodríguez, P., Gristo, P., 2023. Offshore Uruguay: Big Hopes (and Supporting Geology) for the Cretaceous. *First Break* 41, 45–47. <https://doi.org/10.3997/1365-2397.fb2023071>
- de Santa Ana, H., 1989. Consideraciones tectonicas y deposicionales de la Cuenca Norte Uruguaya. *Boletín Tecnico de ARPEL* 18 (4), 319–339.

- de Santa Ana, H., Veroslavsky, G., 2003. La tectosecuencia volcanosedimentaria de la Cuenca Norte de Uruguay. Edad Jurásico-Cretácico Temprano. In: Veroslavsky, G., Ubilla, M., Martínez, S. (Eds.), Cuencas Sedimentarias de Uruguay: Geología, Paleontología y Recursos Naturales. Mesozoico. DI.R.A.C., Montevideo, pp. 5174.
- Duvall, A.R., Tucker, G.E., 2015. Dynamic Ridges and Valleys in a Strike-Slip Environment. *JGR Earth Surface*. <https://doi.org/10.1002/2015jf003618>
- Fontainha, M.V.F., Trouw, R.A.J., Dantas, E.L., Polo, H.J.O., Serafim, I.C.C.O., Furtado, P.C., Negrão, A.P., 2021. Reactivated shear zones: A case study in a tectonic superposition zone between the Southern Brasília and Ribeira orogens, southeastern Brazil. *Journal of South American Earth Sciences*. <https://doi.org/10.1016/j.jsames.2021.103537>
- Garzanti, E., Dinis, P., Vezzoli, G., Borromeo, L., 2021. Sand and mud generation from continental flood basalts in contrasting landscapes and climatic conditions (Paraná–Etendeka conjugate igneous provinces, Uruguay and Namibia). *Sedimentology*. <https://doi.org/10.1111/sed.12905>
- Giona Bucci, M., Schoenbohm, L.M., 2022. Tectono-Geomorphic Analysis in Low Relief, Low Tectonic Activity Areas: Case Study of the Temiskaming Region in the Western Quebec Seismic Zone (WQSZ), Eastern Canada. *Remote Sensing* 14, 3587. <https://doi.org/10.3390/rs14153587>
- Gomes, A.S., Vasconcelos, P.M., 2021. Geochronology of the Paraná–Etendeka large igneous province. *Earth-Science Reviews*. <https://doi.org/10.1016/j.earscirev.2021.103716>
- Heron, P.J., Pysklywec, R.N., Stephenson, R., 2016. Lasting mantle scars lead to perennial plate tectonics. *Nat Commun*. <https://doi.org/10.1038/ncomms11834>
- Holtmann, R., Cattin, R., Simoes, M., Steer, P., 2023. Revealing the hidden signature of fault slip history in the morphology of degrading scarps. *Sci Rep* 13. <https://doi.org/10.1038/s41598-023-30772-z>
- Horton, B.K., 2018. Tectonic Regimes of the Central and Southern Andes: Responses to Variations in Plate Coupling During Subduction. *Tectonics* 37, 402–429. <https://doi.org/10.1002/2017tc004624>
- IDEuy, Instituto Nacional de Estadística, Ministerio de Transporte y Obras Públicas, Dirección Nacional de Topografía (Uruguay, 2018); [https://visualizador.ide.uy/ideuy/core/load\\_public\\_project/ideuy/](https://visualizador.ide.uy/ideuy/core/load_public_project/ideuy/)

- Karson, J.A., Farrell, J.A., Chutas, L.A., Nanfито, A.F., Proett, J.A., Runnals, K.T., Sæmundsson, K., 2018. Rift-Parallel Strike-Slip Faulting Near the Iceland Plate Boundary Zone: Implications for Propagating Rifts. *Tectonics* 37, 4567–4594. <https://doi.org/10.1029/2018tc005206>
- Kirkpatrick, H.M., Moon, S., Yin, A., Harrison, T.M., 2020. Impact of fault damage on eastern Tibet topography. *Geology*. <https://doi.org/10.1130/g48179.1>
- Kröhling, D., Brunetto, E., Galina, G., Zalazar, M.C., Iriondo, M., 2014. Planation Surfaces on the Paraná Basaltic Plateau, South America. *Gondwana Landscapes in southern South America*. [https://doi.org/10.1007/978-94-007-7702-6\\_10](https://doi.org/10.1007/978-94-007-7702-6_10)
- Li, X., Pierce, I.K.D., Ai, M., Luo, Q., Li, C., Zheng, W., Zhang, P., 2022. Active tectonics and landform evolution in the Longxian-Baoji Fault Zone, Northeast Tibet, China, determined using combined ridge and stream profiles. *Geomorphology*. <https://doi.org/10.1016/j.geomorph.2022.108279>
- Li, Y., Liu, M., Zhang, H., Shi, Y., 2021. Stream channel offsets along strike-slip faults: Interaction between fault slip and surface processes. *Geomorphology*. <https://doi.org/10.1016/j.geomorph.2021.107965>
- Manna, M.O., Santos Scherer, C.M. dos, Bállico, M.B., Goso, C.A., Kifumbi, C., Schaffer, G., Toledo, J.C., Ferrari, L.A.B., Ataide Ribeiro dos Santos, A., da Silva Schmitt, R., 2025. Paleoenvironmental reconstruction and stratigraphic implications of the Middle to Late Permian Yaguarí Formation, Norte Basin, Uruguay. *Journal of South American Earth Sciences*. <https://doi.org/10.1016/j.jsames.2025.105381>
- Marliyani, G.I., Arrowsmith, J.R., Whipple, K.X., 2016. Characterization of slow slip rate faults in humid areas: Cimandiri fault zone, Indonesia. *JGR Earth Surface* 121, 2287–2308. <https://doi.org/10.1002/2016jf003846>
- Marmisolle, J., Morales, E., Rossello, E., Soto, M., Hernández-Molina, J., 2025. Tectonic evolution of the Atlantic rift, central sector offshore Uruguay. *Tectonophysics*. <https://doi.org/10.1016/j.tecto.2025.230654>
- Marmisolle, J., Veroslavsky, G., de Santa Ana, H., 2016. Depocenters with Potential Preservation of Pre-carboniferous Rocks in Norte Basin (Uruguay). *International Conference and Exhibition, Barcelona*, pp. 18–20. <https://doi.org/10.1190/ice2016-6337268.1>

- Milani, E.J., De Wit, M.J., 2008. Correlations between the classic Paraná and Cape–Karoo sequences of South America and southern Africa and their basin infills flanking the Gondwanides: du Toit revisited. SP. <https://doi.org/10.1144/sp294.17>
- Mira Carrión, A., Veroslavsky, G., Vives, L., Rodríguez, L., 2016. Influencia de los lineamientos estructurales sobre el flujo del Sistema Acuífero Guaraní en la provincia de Corrientes. *Revista de la Asociación Geológica Argentina*, 73(4), 478–492.
- Moon, S., Perron, J.T., Martel, S.J., Holbrook, W.S., St. Clair, J., 2017. A model of three-dimensional topographic stresses with implications for bedrock fractures, surface processes, and landscape evolution. *JGR Earth Surface* 122, 823–846. <https://doi.org/10.1002/2016jf004155>
- Morales, E., Veroslavsky, G., Manganelli, A., Marmisolle, J., Pedro, A., Samaniego, L., Plenc, F., Umpiérrez, R., Ferreiro, M., Morales, M., 2021. Potential of geothermal energy in the onshore sedimentary basins of Uruguay. *Geothermics* 95, 102165. <https://doi.org/10.1016/j.geothermics.2021.102165>
- Muir, R.A., Whitehead, B.A., New, T., Stevens, V., Macey, P.H., Groenewald, C.A., Salomon, G., Kahle, B., Hollingsworth, J., Sloan, R.A., 2023. Exceptional Scarp Preservation in SW Namibia Reveals Geological Controls on Large Magnitude Intraplate Seismicity in Southern Africa. *Tectonics*. <https://doi.org/10.1029/2022tc007693>
- Muzio, R., Olivera, L., Fort, S., Peel, E., 2022. Petrological features of the first Cenozoic alkaline magmatic event recorded in northwestern Uruguay, southern extreme of the Paraná basin. *Journal of South American Earth Sciences*. <https://doi.org/10.1016/j.jsames.2022.103796>
- Nuñez Demarco, P., Masquelin, H., Prezzi, C., Aífa, T., Muzio, R., Loureiro, J., Peel, E., Campal, N., Sánchez Bettucci, L., 2020. Aeromagnetic patterns in Southern Uruguay: Precambrian-Mesozoic dyke swarms and Mesozoic rifting structural and tectonic evolution. *Tectonophysics*. <https://doi.org/10.1016/j.tecto.2020.228373>
- Oriolo, S., Hueck, M., Oyhantçabal, P., Goscombe, B., Wemmer, K., Siegesmund, S., 2018. Shear Zones in Brasiliano-Pan-African Belts and Their Role in the Amalgamation and Break-Up of Southwest Gondwana. *Regional Geology Reviews*. [https://doi.org/10.1007/978-3-319-68920-3\\_22](https://doi.org/10.1007/978-3-319-68920-3_22)
- Oriolo, S., Oyhantçabal, P., Basei, M.A.S., Wemmer, K., Siegesmund, S., 2016. The Nico Pérez Terrane (Uruguay): From Archean crustal growth and connections with the Congo

- Craton to late Neoproterozoic accretion to the Río de la Plata Craton. *Precambrian Research* 280, 147–160. <https://doi.org/10.1016/j.precamres.2016.04.014>
- Oriolo, S., Oyhantçabal, P., Heidelbach, F., Wemmer, K., Siegesmund, S., 2015. Structural evolution of the Sarandí del Yí Shear Zone, Uruguay: kinematics, deformation conditions and tectonic significance. *Int J Earth Sci (Geol Rundsch)*. <https://doi.org/10.1007/s00531-015-1166-2>
- Panara, Y., Menegoni, N., Finkbeiner, T., Zühlke, R., Vahrenkamp, V., 2024. High-resolution analysis of 3D fracture networks from Digital Outcrop Models, correlation to plate-tectonic events and calibration of subsurface models (Jurassic, Arabian Plate). *Marine and Petroleum Geology*. <https://doi.org/10.1016/j.marpetgeo.2024.106998>
- Panario, D., Gutiérrez, O., Sánchez Bettucci, L., Peel, E., Oyhantçabal, P., Rabassa, J., 2014. Ancient Landscapes of Uruguay. *Gondwana Landscapes in southern South America*. [https://doi.org/10.1007/978-94-007-7702-6\\_8](https://doi.org/10.1007/978-94-007-7702-6_8)
- Pascal, C., 2022. Brittle structures in the field. *Paleostress Inversion Techniques*. <https://doi.org/10.1016/b978-0-12-811910-5.00006-3>
- Passarelli, C.R., Basei, M.A.S., Wemmer, K., Siga, O., Jr, Oyhantçabal, P., 2011. Major shear zones of southern Brazil and Uruguay: escape tectonics in the eastern border of Rio de La plata and Paranapanema cratons during the Western Gondwana amalgamation. *Int J Earth Sci (Geol Rundsch)*. <https://doi.org/10.1007/s00531-010-0594-2>
- Peace, A.L., Jess, S., 2023. Microdrones in field-based structural geology: a photogrammetry and fracture quantification case study from the North Mountain Basalt, Nova Scotia, Canada. *Drone Syst. Appl*. <https://doi.org/10.1139/dsa-2022-0037>
- Pereira-Claren, A., Gironás, J., Niemann, J.D., Passalacqua, P., Mejia, A., Escauriaza, C., 2019. Planform geometry and relief characterization of drainage networks in high-relief environments: An analysis of Chilean Andean basins. *Geomorphology*. <https://doi.org/10.1016/j.geomorph.2019.05.011>
- Porta, F., Spoturno, J., Rossi, P., Heinzen, W., & Ministerio de Industria Energia y Minería, Dirección Nacional de Minería y Geología, Montevideo (Uruguay), 1985. Carta geológica del Uruguay a escala 1:500.000.
- Reitman, N.G., Klinger, Y., Briggs, R.W., Gold, R.D., 2022. Climatic influence on the expression of strike-slip faulting. *Geology* 51, 18–22. <https://doi.org/10.1130/g50393.1>

- Reitman, N.G., Mueller, K.J., Tucker, G.E., Gold, R.D., Briggs, R.W., Barnhart, K.R., 2019. Offset Channels May Not Accurately Record Strike-Slip Fault Displacement: Evidence From Landscape Evolution Models. *JGR Solid Earth*. <https://doi.org/10.1029/2019jb018596>
- Rimando, J.M., Peace, A.L., 2021. Reactivation Potential of Intraplate Faults in the Western Quebec Seismic Zone, Eastern Canada. *Earth and Space Science*. <https://doi.org/10.1029/2021ea001825>
- Rodríguez, P., Marmisolle, J., Soto, M., Gristo, P., Benvenuto, A., de Santa Ana, H., Veroslavsky, G., 2015a. Preliminary results of new gravity surveys onshore Uruguay, with a 2D modeling case study from Norte Basin. *SEG Technical Program Expanded Abstracts 2015*. <https://doi.org/10.1190/segam2015-5814479.1>
- Rodríguez, P., Veroslavsky, G., Soto, M., Marmisolle, J., Gristo, P., de Santa Ana, H., Benvenuto, A., 2015b. New integrated Bouguer gravity anomaly map onshore Uruguay: preliminary implications for the recognition of crustal domains. *SEG Technical Program Expanded Abstracts 2015*. <https://doi.org/10.1190/segam2015-5821993.1>
- Salomon, E., Koehn, D., Passchier, C., 2015a. Brittle reactivation of ductile shear zones in NW Namibia in relation to South Atlantic rifting. *Tectonics*. <https://doi.org/10.1002/2014tc003728>
- Salomon, E., Koehn, D., Passchier, C., Hackspacher, P.C., Glasmacher, U.A., 2015b. Contrasting stress fields on correlating margins of the South Atlantic. *Gondwana Research*. <https://doi.org/10.1016/j.gr.2014.09.006>
- Sánchez Bettucci, L., Kacevas, M.R., Castro, H., Olivet, J.L., Latorres, E., 2025. Summary of the intracontinental seismicity of Uruguay. *Journal of South American Earth Sciences* 161, 105578. <https://doi.org/10.1016/j.jsames.2025.105578>
- Sánchez Bettucci, L., Loureiro, J., Castro, H., Rodrigues, M., Dell'Acqua, D., Latorres, E., Curbelo, A., 2021a. Informe de Evento UY05082021 - Florida. *OGU Informes de Eventos*. OGU, Montevideo, p. 5.
- Scherer, C.M.S., Reis, A.D., Horn, B.L.D., Bertolini, G., Lavina, E.L.C., Kifumbi, C., Goso Aguilar, C., 2023. The stratigraphic puzzle of the permo-mesozoic southwestern Gondwana: The Paraná Basin record in geotectonic and palaeoclimatic context. *Earth-Science Reviews*. <https://doi.org/10.1016/j.earscirev.2023.104397>
- Tibaldi, A., Corti, N., De Beni, E., Bonali, F.L., Falsaperla, S., Langer, H., Neri, M., Cantarero, M., Reitano, D., Fallati, L., 2021. Mapping and evaluating kinematics and the stress and

strain field at active faults and fissures: a comparison between field and drone data at the NE rift, Mt Etna (Italy). *Solid Earth*. <https://doi.org/10.5194/se-12-801-2021>

Tucker, G.E., Hobbey, D.E.J., McCoy, S.W., Struble, W.T., 2020. Modeling the Shape and Evolution of Normal-Fault Facets. *JGR Earth Surface* 125. <https://doi.org/10.1029/2019jf005305>

Veroslavsky, G., Aubet, N., Martínez, S.A., Heaman, L.M., Cabrera, F., Mesa, V., 2019. Late Cretaceous Stratigraphy Of The Southeastern Chaco - Paraná Basin ("Norte Basin" - Uruguay): The Maastrichtian Age Of The Calcification Process. *Geociencias*. <https://doi.org/10.5016/geociencias.v38i2.13779>

Veroslavsky, G., de Santa Ana, H., Goso, C. & Gonzalez, S., 1997. Calcretas y silcretas de la región oeste Uruguay (Queguay), cuenca de Paraná (Cretácico Superior - Terciario Inferior). *Geociencias*, 16(1), pp.205–224.

Veroslavsky, G., Rossello, E.A., López-Gamundí, O., de Santa Ana, H., Assine, M.L., Marmisolle, J., de J Perinotto, A., 2021. Late Paleozoic tectono-sedimentary evolution of eastern Chaco-Paraná Basin (Uruguay, Brazil, Argentina and Paraguay). *Journal of South American Earth Sciences*. <https://doi.org/10.1016/j.jsames.2020.102991>

Veroslavsky, G., Soto, M., Mesa, V., Manganelli, A., 2024. Geology of the Guaraní Aquifer System in the outcrop area of the Tacuarembó and Rivera formations (Norte Basin, Uruguay). *Revista de la Asociación Geológica Argentina*, 81(2), 239–264.

Walker, R.J., Holdsworth, R.E., Armitage, P.J., Faulkner, D.R., 2013. Fault zone permeability structure evolution in basalts. *Geology* 41, 59–62. <https://doi.org/10.1130/g33508.1>

Woodcock, N.H., Mort, K., 2008. Classification of fault breccias and related fault rocks. *Geol. Mag.* <https://doi.org/10.1017/s0016756808004883>

Zhou, R., Schoenbohm, L.M., Cosca, M., 2013. Recent, slow normal and strike-slip faulting in the Pasto Ventura region of the southern Puna Plateau, NW Argentina. *Tectonics* 32, 19–33. <https://doi.org/10.1029/2012tc003189>